

## FPIV Study of Density Effect on Air Entrainment In Gasoline Dense Sprays

Brice Prosperi<sup>1</sup>, Jérôme Helie<sup>2</sup> and Rudy Bazile<sup>1</sup>

1: Institut de Mécanique des Fluides de Toulouse, 31400 Toulouse, France, prosperi@imft.fr

2: Siemens VDO Automotive BP1149, 1 av. Paul Ourliac, 31036 Toulouse cedex 1, France, jerome.helie@siemens.com

---

**Abstract** Air entrainment in high pressure piezoelectric injector for gasoline direct injection is studied by mean of Fluorescent Particle Image Velocimetry. A combination of PIV data filtering is proposed as an efficient way to eradicate dubious vectors remaining inside the dense spray due to Mie scattering by the liquid phase. Analyses are performed on mean average velocity flow fields obtained with long time injection duration and various ambient pressures up to 15 bar. The vessel being limited at 12 bar maximum relative pressure, a dense gas CF<sub>4</sub> is used to simulate higher pressure. Density effect on air entrained by the spray is analyzed leading to the distinction between the air entrainment region and the vortex one. A direct method for air entrained mass flow rate is used, enabled by the availability of velocity vectors very close to the spray edge. Density effect on air entrainment in quasi steady region is analyzed leading again to the differentiation of a near zone and a far one. Whereas spray better entrains air for high ambient density, a common trend is observed. In the near field, the cumulative air entrained mass flow rate follows a 3/2-power law whereas, in the far field, a linear dependence of entrained mass flow rate as a function of axial distance is found. Then, an integral model for full cone spray is used to compare experimental results. As good agreement was found, a physical analysis is proposed to better appreciate the model's prediction of air entrained in the quasi-steady region. Further works are still in progress to study the interaction of the unsteady vortex with the surrounding gas.

---

### 1. Introduction

Due to the necessary reduction of pollutants emission, automotive manufacturers have to product more efficient and cleaner engines. During the late nineties, a new generation of engine technology (direct injection) appeared on the market. First homogeneous then stratified Gasoline Direct Injection (GDI) strategies were proposed to improve fuel saving for engines by mean of a better combustion. Indeed, an efficient way of operating a gasoline internal combustion is to burn the fuel in an air excess.

The first generation, so called "wall guided", used a combination of both shaped piston bowl and intake valves to transport a kernel of stoichiometric, or rich, air / fuel mixture towards the spark plug, remaining the overall mixture in the whole combustion chamber globally lean. The application of this stratified GDI strategy reached its limits for very small injected quantities because of over-mixing. The second generation is based on a stratification of a fuel quantity directly formed by the spray itself which is oriented through the ignition point of the spark. The efficiency of the "spray guided" strategy depends on the ability of controlling the mixture concentration's area in function of the engine conditions. Well-established strategy for stratified spray guided GDI combustion has not yet been found, however, first investigations [1] showed that the injection conditions such as injection timing, injection pressure, aerodynamics (spray interactions with surrounding air [2]), piston design and spray characteristics have to be optimized to control the mixture formation [3].

This experimental work is carried out in the continuity of the researches engaged at IMFT [4], whose objective was to study the air entrainment process induced by GDI dense spray (figure 2) and to estimate the impact on air / fuel mixture formation [5]. An adaptation of the application of Particles Image Velocimetry (PIV) has been developed [6] in order to measure the air entrainment

of dense two phase-flows. This method consists in replacing “classic” PIV tracer particles by fluorescent ones. By mean of Fluorescence Particles Image Velocimetry (FPIV) technique, measurements [7] can be made very close to the spray edge. Therefore, air velocity measurements are achieved and used to compute the air mass flow rate entrained by the unsteady spray.

After a description of recent development [8] of the FPIV post processing, the validation of mean flow field calculation is presented. The density effect of air entrained mass flow rate is presented. The axial evolution of the air mass flow rate entrained by a hollow cone spray in the quasi-static region is discussed as well as the effects of ambient pressure. In order to complete the physical analysis of density effect, an integral model [9] for air entrainment in axisymmetric full cone spray is used. Then, future works are presented.

## 2. Experimental Setup

### 2.1 Injection bench

The high pressure direct injection system [10] has been designed at IMFT initially to study the influence of pulsed flow on the liquid mass flow rate at injector's outlet. To perform this task in respect of real vehicle conditions, Siemens VDO automotive (SV) components have been implemented such as high pressure gasoline fuel pump, pressure regulator, common rail and piezoelectric injector. Taking experience from previous studies, modifications have been made to improve the injection bench in terms of control and flexibility.

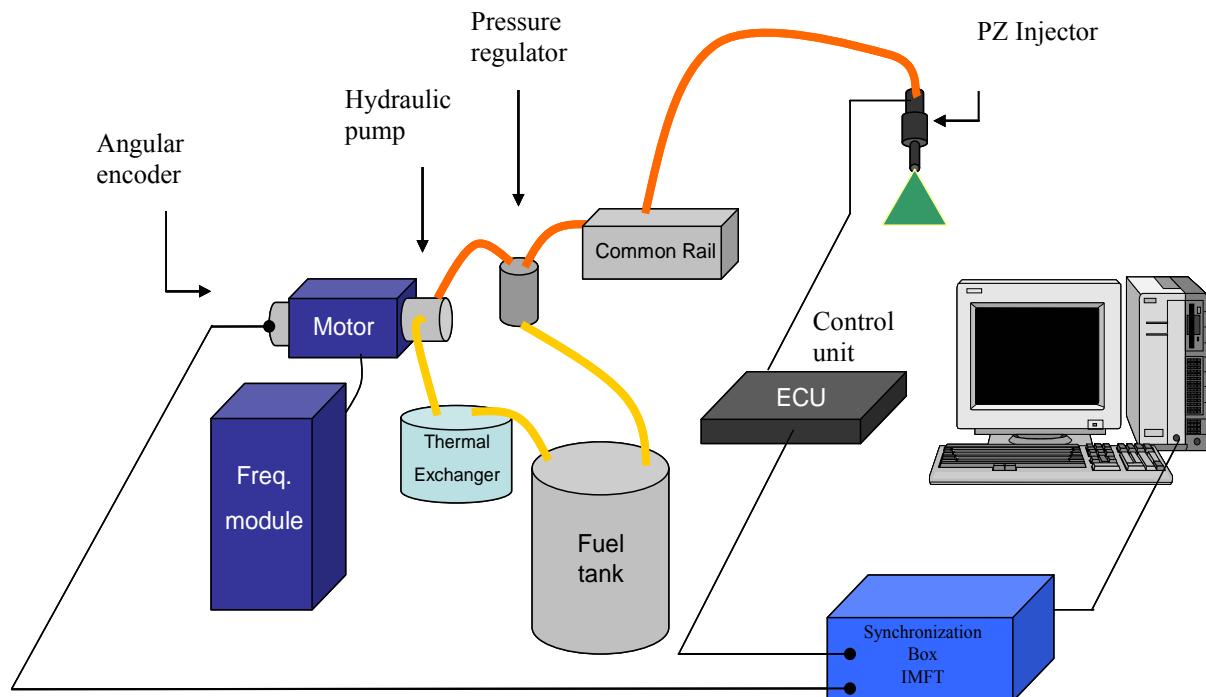


**Figure 1 : High pressure gasoline direct injection bench**

The hydraulic pump is entrained by an asynchronous motor. To allow for operation at speeds up from range 600 rpm to 3000 rpm, a frequency modulator has been added. To ensure the well synchronization between injections and 3-pistons pump's motions, a 10bit resolution angular encoder has been mounted on the end the motor's shaft.

The liquid used is a non-evaporating iso-paraffin, called Isane IP 155, with physical properties close to gasoline's. Due to close loop condition, the liquid is ensured remaining at constant temperature (303 K) by circulating through thermal exchanger implemented upward the hydraulic pump. Then liquid is compressed up to 220 bars. To reduce pressure fluctuations inside the system,

a bulky common rail of 250 cc, equipped with pressure sensor, accumulate pressurized liquid. Injection pressure ( $P_{INJ}$ ) is regulated in the range 50 bar to 200 bars.

The gasoline direct injector has been mounted on the top of the chamber down forward and is driven by a SV electronic control unit (ECU). Manual switches permit to control the activation's power of piezoelectric component and implicitly the needle lift around its nominal position (26  $\mu\text{m}$ ). The needle reaching the desired position in a delay of 100 $\mu\text{s}$  approximately, the pulse width (PW) duration will be taken in the range 0.2 ms to 1.5ms. The outward opening injector generates a 80° hollow cone spray (figure 2) thanks to its annular shaped orifice (4,2mm diameter). This injector has been improved in terms of engine stability, life durability, size and cost reduction.

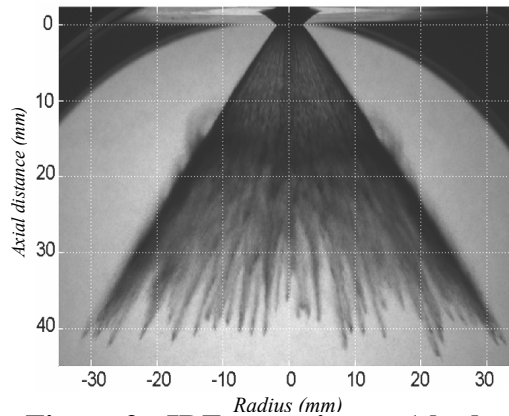


**Figure 2 : IDE spray image (shadowgraphy)**

The modification made on the setup increased the accuracy of the studied system and permit to control injections with less than 1% pressure fluctuation.

## 2.2 FPIV configuration

As our interest is to analyze instantaneous velocity field of the air entrainment of the spray (by PIV), we have to keep in mind that video sensor can be damaged while dense liquid area is illuminated. Thus, we use here the Particle Image Velocimetry on Fluorescent dye (FPIV) as a mean of investigation [6]. The high pressure GDI bench is tested on experimental setup for air entrainment analysis as illustrated in figure 3.

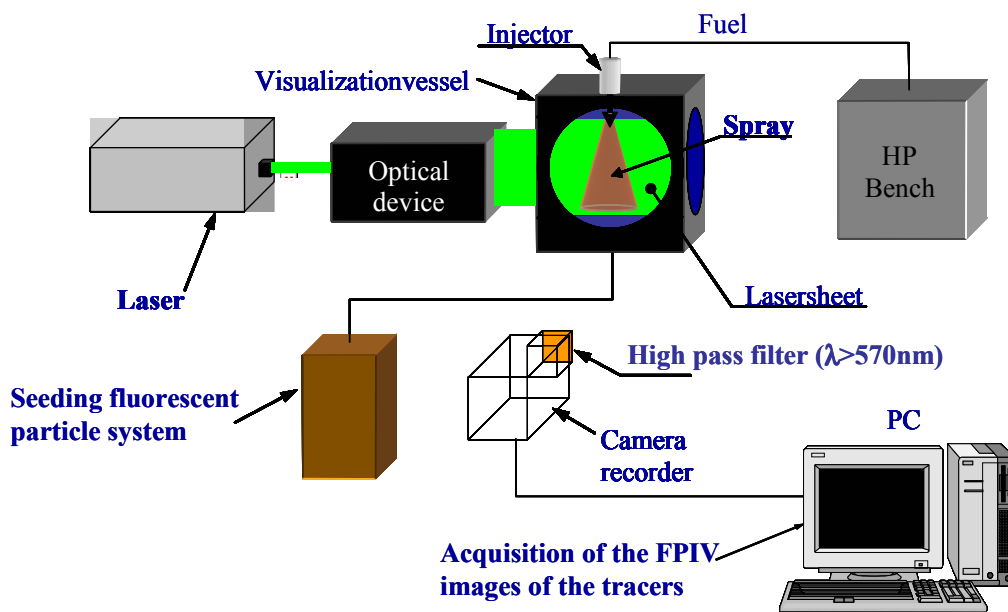


**Figure 3 : Experimental set-up for FPIV**

The injections were carried out in a pressurized chamber (up to 1.2MPa) with appropriate 110 mm optical accesses. The vessel is equipped with pressure and temperature sensors for ambient condition control. The effect of density is studied by inflating the chamber up to a desired pressure either with air or with another gas. Using dense tetrafluoromethane (CF<sub>4</sub>) gas, whose density is three times higher than air, permits to reach air equivalent density in the range 1,2 to 43,2 kg/m<sup>3</sup>.

To establish a continuous flow of fluorescent tracers inside the chamber, the gas is passing through a medical atomizer full of a propylene carbonate (PC) solution saturated with dichloromethane (DCM). The dye particles generated, whose mean diameter is close to 0.8μm with a sharp repartition around it, have interesting fluorescent properties. Indeed, when excited by a Nd:Yag laser light of 532 nm wavelength (second harmonic), the particles emit a broadband fluorescent emission between 615 and 666 nm, a peak of efficiency being noticed at 639 nm wavelength. The tracers concentration inside the bomb is controlled by opening valves duration upstream and downstream the atomizer and ensures quite good reproduction series from one seeding to another.

The excitation source is a Spectra Physics double-pulse laser with a beam waist of the order of 300μm and an intensity of 2\*200 mJ. The beam is passing through convergent then divergent lens generating a laser sheet in the vertical symmetry plane of the injector. In order to filter the Mie-scattering of the laser by the liquid sheet, a high pass filter ( $\lambda > 570$  nm) is placed in front of the camera recorder (Sensicam CCD sensor 1280\*1024 pixels with a Nikon lens). However, due to the low energy of the fluorescence signal, 2 per 2 binning pixel were used, reducing the resolution but allowing higher framing rate and increasing the sensor sensibility. Taking into account the axial symmetry property, the view field of the camera is adjusted on the half size of the spray (30\*40 mm<sup>2</sup>).

The experimental setup is driven by a personal computer so that laser shots and images acquisitions are synchronized and triggered by injections. The synchronization box, designed at IMFT, permits to control single injections as well as double injections via various parameters: frequency, number, PW and inter shot duration.

### **3. Velocity flow field of entrained gas**

#### **3.1 Instantaneous velocity field**

The PIV algorithm is a multipass cross correlation based one with sub pixel cell shifting and grid deformation [11] [12]. Interrogation cells size is 16\*16 pixels<sup>2</sup> with 50% overlap, the actual size of PIV cells being then 900\*900μm<sup>2</sup>. The delay between pulses,  $\Delta t$ , has been taken equal to 15μs for long injection duration and 20μs for shorter one.

In the observed flow region, both liquid and gaseous phases are present and associated with high and low velocity, respectively, with one order difference of magnitude. At the nominal injection pressure of 200 bar, the spray is so dense that the gas flow velocity field is not accessible inside the spray due to a strong Mie scattering of fluorescent light by the liquid sheet.

Traditional PIV algorithm, applied on the overall dense two-phases flow field, does not differentiate tracers and small contributions from the liquid phase, that can lead to spurious vectors inside the spray. This is the reason why post treatment of FPIV data has been improved to better detect wrong one (figure 4-a).

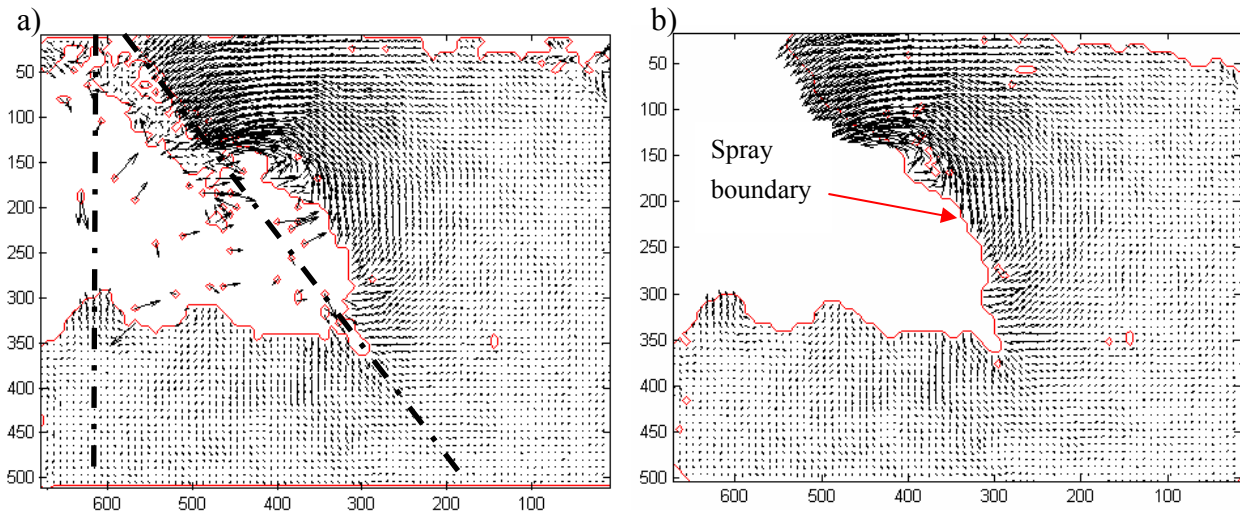


**Figure 4 : Instantaneous velocity flow field in pixel unit ( $P_{inj}=200\text{bar}$ ,  $P_c=10\text{bar}$ ,  $t_{aso}=0.50\text{ms}$ ) : classic filtering (a), two-phase flow filtering (b)**

A generalization of the original median test, relying on a median residual's normalization, has recently been proposed by Westerweel [8]. This test presents the advantage of a single detection threshold (value of about 2) and permits to reject part of wrong measurement data. As used in combination (figure 5) with traditional tests (module,  $|U|$ , and signal noise ratio, SNR), the normalized median test (NMT) has been slightly modified to take into account only remaining vectors after the previous tests. The last persistent wrong isolated vectors are eliminated thanks to a logical test based on the number of direct valid/true neighbors (TN).

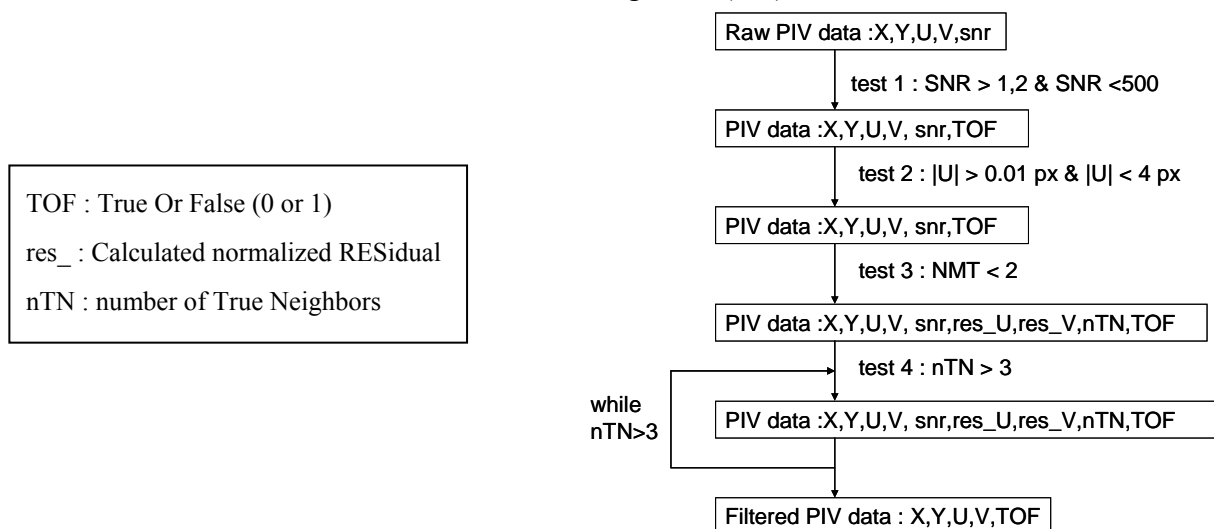


**Figure 5 : FPIV filtering algorithm**

The method used for outlier detection has been tested on each instantaneous dense two phases flow field and seems very stringent (figure 4-b).

### 3.2 Mean velocity field

The FPIV post processing method permits to eradicate a maximum of spurious instantaneous vectors but some, inside of the spray, remain and could bias the mean averaged flow field. Their persistence is due to their gathering as well as their low magnitude so that the median residual test did not detect them. Outside of the spray, the methodology has been evaluated in terms of mass balance error and its convergence. In respect of the current methodology, a minimum number of 20 samples is needed for a maximum 5% error acceptance [4].

By the same way, this threshold also permits to avoid residual persisting wrong vectors inside the spray. The visualization of validated area (figure 6) permits to identify part of the field where the number of valid vector is reduced (such as the contours of the spray as well as the optical window borderline). Concerning the spray, geometrical fluctuations can be observed that take into account both cycle to cycle variations and unsteady effects.

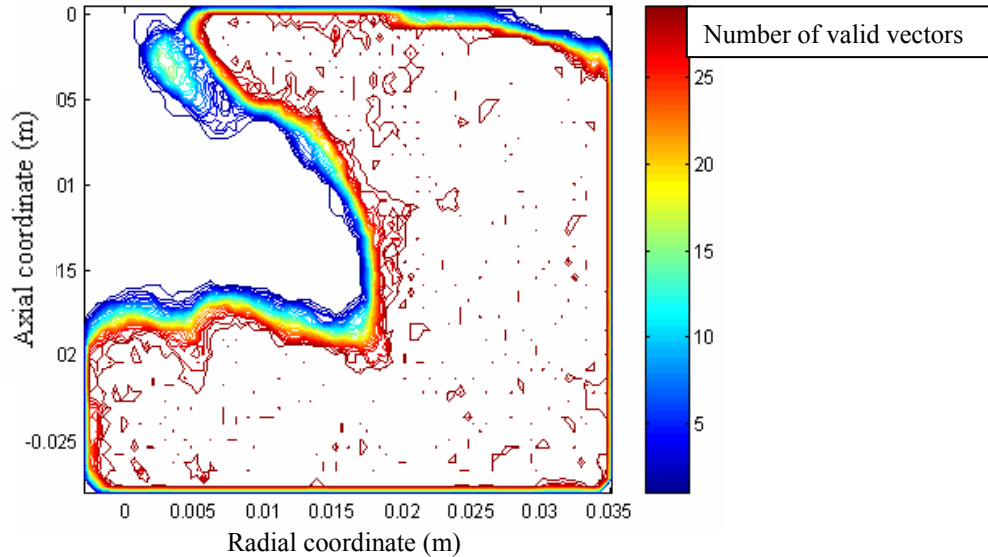


**Figure 6 : Number of local valid vector**

### 3.3 Air entrainment calculation

FPIV allows velocity measurement very close to the spray edge, the distance being less than 1 millimeter. Direct method for entrainment calculation can be applied thanks to a well defined conical surface control. The cumulated mass flux of entrained air along the calculation surface between axial locations  $Z_1$  and  $Z_2$  is given by:

$$\dot{m}_e = \int_{Z_1}^{Z_2} \rho \vec{U} \cdot \vec{n} 2\pi r \frac{dz}{\cos \frac{\theta_s}{2}} = \int_{Z_1}^{Z_2} \rho U_n 2\pi r \frac{dz}{\cos \frac{\theta_s}{2}} \quad \text{with} \quad \vec{U} \cdot \vec{n} = U_n = \|\vec{U}\| \sin \left( \arctan \left( \frac{U}{V} \right) - \left( \frac{\pi}{2} + \frac{\theta_s}{2} \right) \right)$$

with  $\vec{U}$ , the mean averaged velocity vector and  $\theta_s$ , the cone angle.

Normal and tangential velocity decomposition is useful to compute mass flux through control surface (figure 7) defined by half angle spray ( $\theta_s / 2 = 40^\circ$ ). It also permits to check vector's direction.

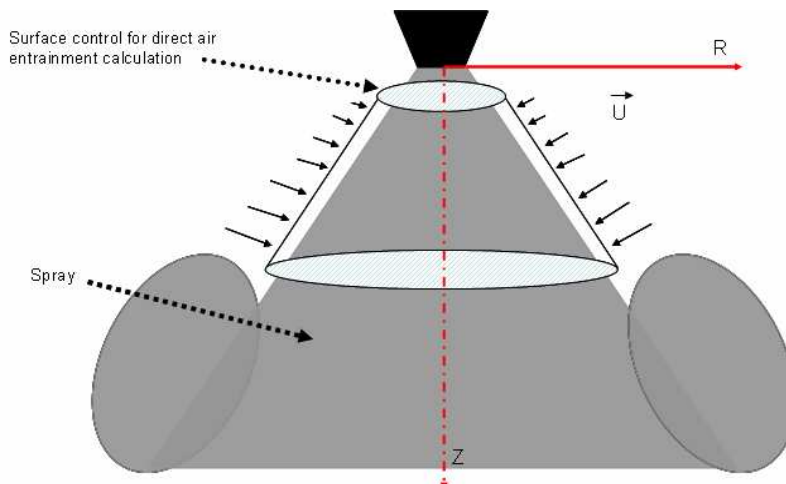


**Figure 7 : Direct air entrainment calculation**

## 4. Mass flow rate of entrained gas in the quasi static region

### 4.1 Typical result at ambient pressure

First considerations concerned 80° hollow cone spray results obtained at ambient density for an injection frequency of 10Hz, injection pressure of 200 bars, pulse width of 1,5 ms and medium lift (~30 μm). The air entrainment governing parameters are liquid sheet thickness (>20μm) and liquid velocity at the injector nozzle (>100m/s). The Sauter Mean Diameter (SMD) of atomized droplets produced by PZ injector is close to 10 μm. To ensure the area of interest to be quasi steady, observation timing is taken long enough after start of injection (aso<sub>i</sub>) and a few hundred microseconds before the end of injection. Air entrained mass flow rate is calculated from velocity profile at a distance of 1 mm from spray frontier (A).

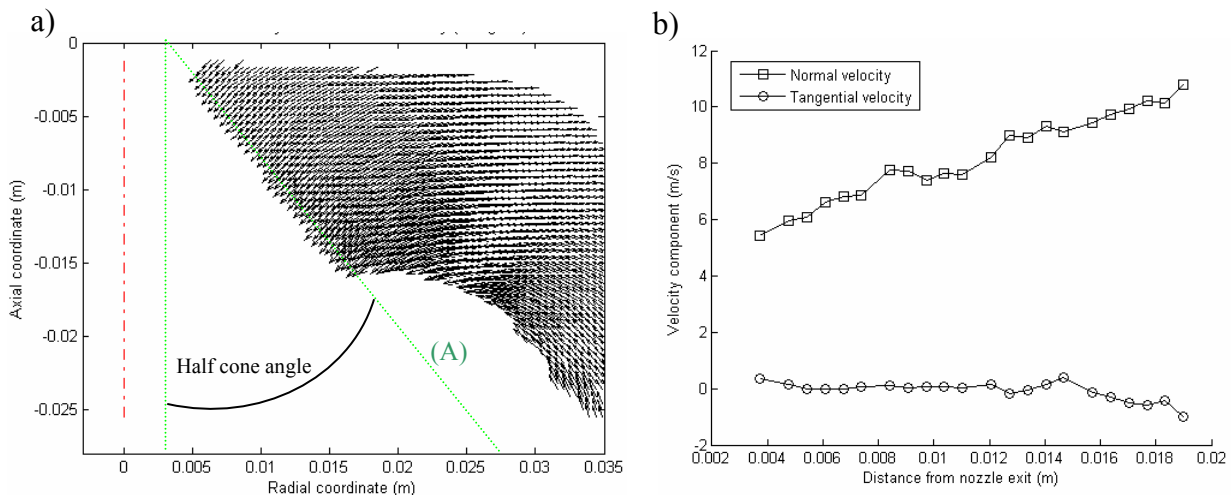


Figure 8-a : Mean flow velocity field.

Figure 8-b : Normal ( $U_n$ ) and tangential ( $U_t$ ) velocity components along (A).

As can be observed in figure 8-a, air is strongly sucked toward the spray in the vicinity of the injector outlet whereas, "far away" from this region, global air motion is rotating. This observation permits to distinguish two different zones that are the quasi steady air entrainment area (I) and unsteady vortex area (II), respectively. A closer look at normal and tangential velocities is of a great help in the physical analysis. Whereas normal velocity increases with axial distance (figure 8-b), tangential one remains close to zero until  $Z = 14$  mm. This indicates that air velocity vectors are directed orthogonally to the spray and that air is sucked progressively reaching a maximum entrainment velocity just before area (II). Negative values of tangential velocities, indicates that air velocity vectors are oriented through injection direction.

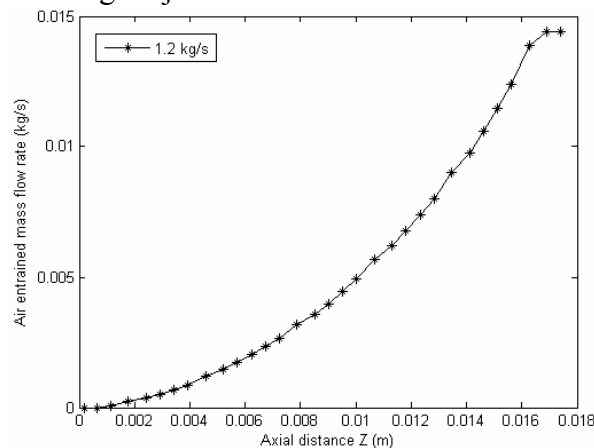
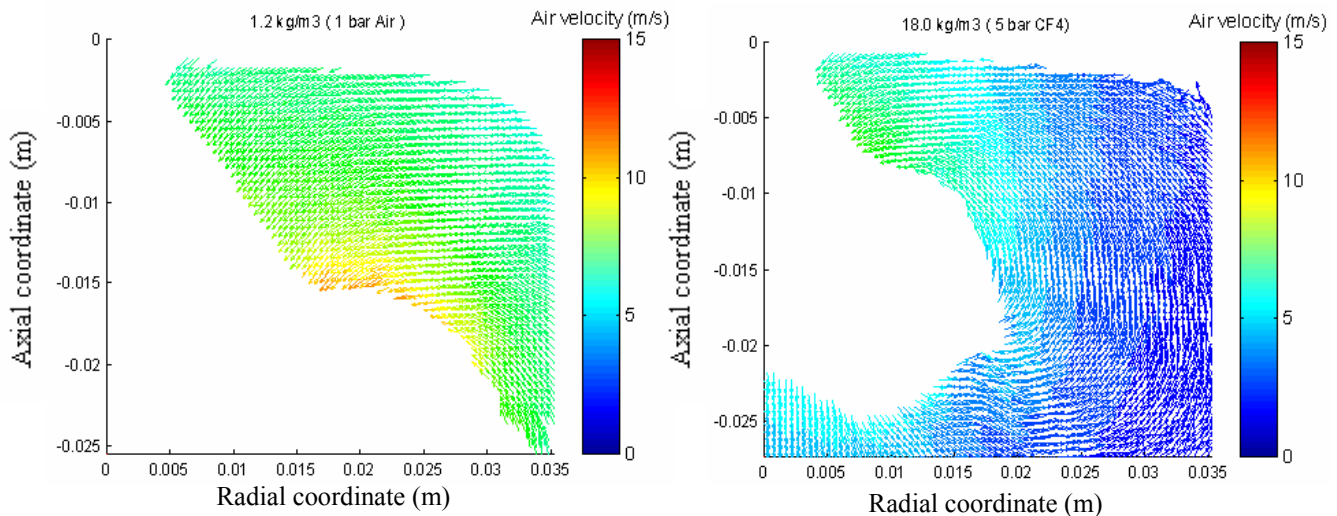


Figure 9: Cumulative air mass flow rate  $\dot{m}_e$  along (A).

Cumulative air entrained mass flow rate through the surface control defined by the axis revolution of (A) (figure 9) can be plotted. In region (I),  $\dot{m}_e$  is found to increase non linearly with axial distance  $Z$  as established for gaseous variable density jets. Inside the vortex zone, normal velocity decreases so that an inflexion point on  $\dot{m}_e$  should be observed for higher value of  $Z=16$  mm.

#### 4.2 Density effect on air entrainment

Engine conditions impose high back pressure during the injections. Therefore, density effect has been investigated keeping constant the other injection parameters. As described in section 2.2, CF4 is used to reach high density. Figure 10 shows that the spray penetration is strongly reduced at 18 kg/m<sup>3</sup> compared with lower density, momentum exchange between droplets and gas being enhanced at high density.



**Figure 10 : Mean velocity flow field of entrained gas at various density.**

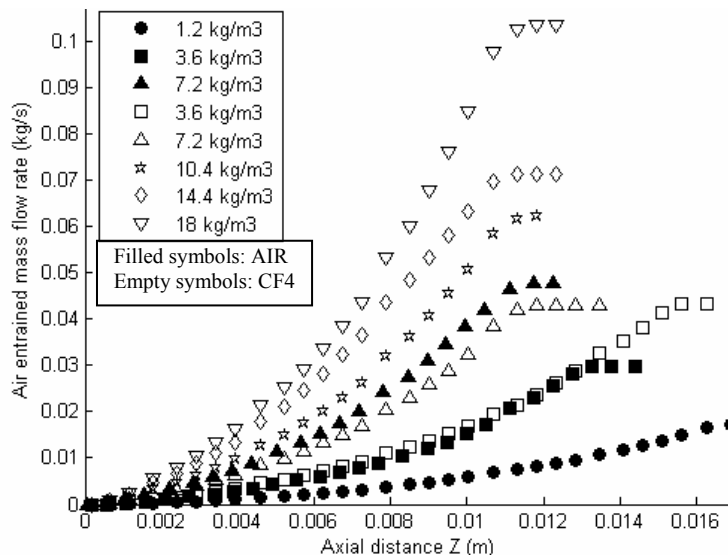


**Figure 11 : Cumulative air entrained mass flow rate at various ambient density.**

As can be seen on figure 11 the denser the environment is, the more the surrounding gas will interact with the fuel droplets without apparent effect of saturation. The increase in the cumulative mass flow rate of entrained gas between the extreme cases ( $\rho = 1.2$  kg/m<sup>3</sup> and  $\rho = 18$  kg/m<sup>3</sup>) is about 1200 %. Furthermore, results at same density (3.6 and 7.2 kg/m<sup>3</sup>) using AIR and CF4 are in

good agreement as expected. The small differences between AIR and CF4 come from the difficulty of filling the pressurized chamber strictly with the CF4 gas whereas purge is performed with air. However, a particular care will be taken for further experiments. Whatever the ambient density, a common trend is appearing on air entrainment curves. However, it is easily observed that gas is better entrained when ambient density is high.

### 4.3 Integral model

These results successfully match previsions from Cossali's model [9] in function of the axial location and ambient density (figure 12). The model is a one-dimensional one for predicting gas entrainment into a non-evaporating full cone steady spray injected into a stagnant gas at uniform pressure. Based on mass conservation and momentum balance, a law relating the entrained mass flow rate is formulated. As droplets drag force is supposed to be the main mechanism, the entrained mass flow rate depends on the distance from the nozzle and can be split into two entrainment distinct regions (for example, point A<sub>18</sub> for 18 kg/m<sup>3</sup> ambient density). In the near field, the cumulative air entrained mass flow rate follows a 3/2-power law whereas in the far field the linear dependence of entrained mass flow rate on nozzle distance (like in gaseous jet) is recovered. Although model has been developed for full cone spray, the same assumptions can be done for the hollow cone spray so that satisfying comparisons are found between analytical and experimental data.

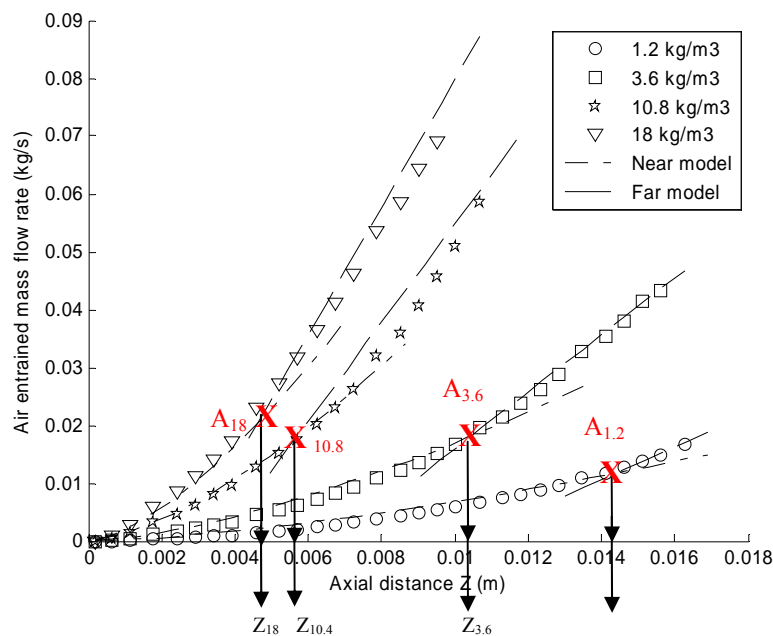


**Figure 12 : Superimposition of experimental and analytical results**

Gathering constants of the model in symbol  $\alpha$ , near and far field models can, respectively, be expressed like:

$$\dot{m}_e(z \rightarrow z_0) \approx \alpha_n \left( \frac{\rho_g}{\rho_0} \right)^{5/6} z(z - z_0)^{1/2}$$

$$\dot{m}_e(z \gg z_0) = \alpha_f \left( \frac{\rho_g}{\rho_0} \right)^{1/2} z$$

The near  $\alpha_n$  and far  $\alpha_f$  coefficients are fitted according to case at higher pressure (18 kg/m<sup>3</sup>) and are found to be 5,8 and 2,6, respectively. These coefficients stand for part of the slope's stiffness in addition to density ratio power law. The fictiv origin  $z_0$  is taken as primary atomization length and is about 1 mm. However, this length is function of initial liquid velocity as well as liquid sheet

thickness which strongly depends on internal geometry of shaped injectors.

Another observation concerns the transition point ( $A_{1.2}$ ,  $A_{3.6}$ ,  $A_{10.8}$ ,  $A_{18}$ , respectively 1.2, 3.6, 10.8 and 18 kg/m<sup>3</sup>) between near and far model which is discussed in the next part.

#### 4.4 Analysis of the density effect

First remark concerns the location of transition point  $A_i$ , defined as near / far transition point for ambient density "i". The more the ambient density is, the sooner the linear dependence of entrained air as a function of axial distance is recovered (as in gaseous jet). Downward this transition point, a 3/2-power law dependence of cumulative air entrained mass flow rate is found. This can be interpreted by the difference of liquid phase concentration. Indeed, at the injector's outlet, spray is dense like a liquid sheet whereas far away, droplet dispersion leads to a more dilute spray. This implies a difference in gas / liquid aerodynamics interaction. The distinction between zone (I) and (II) is difficult to appreciate however the boundary layer seems being recognized (figure 13).

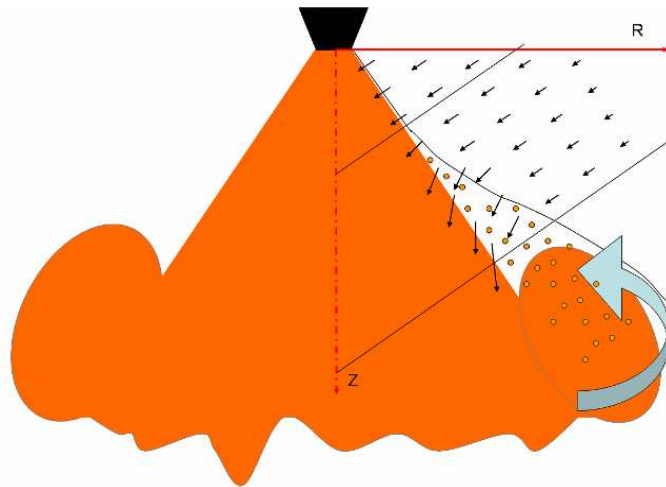


Figure 13 : Schematic representation of boundary layer surrounding the spray.

The access of velocity profiles inside the boundary layer, in particular the tangential velocity, permits to evaluate the axial location of transition point at various ambient densities (figure 14). Reporting inflexion point on tangential velocity, a rapid decrease of  $A_i$  location in function of gas density is observed.

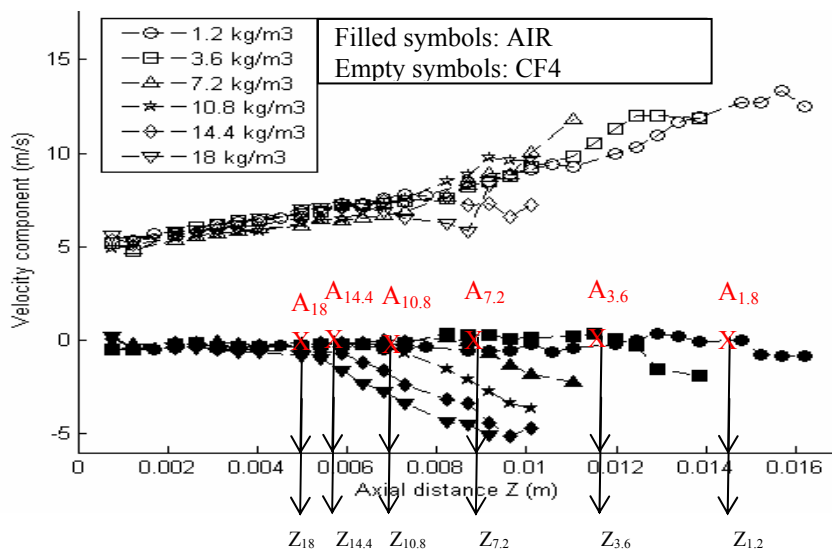


Figure 14 : Normal and tangential velocity profile near spray axis (left). Density Effects on transition point.

In order to perform a physical analysis trying to explain the previous observation, a characteristic length  $L_{\tau p}$  being the product of initial liquid velocity  $U_0$  ( $\sim 100$  m/s) by the droplet time response  $\tau_p$  (table 1) is calculated. Taken Malvern Spraytec measurement of spray droplet's size, an estimation of the droplet time response is done. Empirical relation based on spherical isolated particle is used:

$$\tau_p = \frac{\rho_p d_p^2}{18\mu_f} \left[ 1 + \frac{Re_p^{0.66}}{6} \right] \quad (Re_p < 1000)$$

$$\text{With } Re_p = \frac{\rho_f U_{rel} D_d}{\mu_f}$$

rho_g (kg/m3)	1,2	3,6	7,2	10,8	14,4	18
Rep	14,4	43,2	86,4	129,6	172,8	216
Tp ( $\mu$ s)	308	200	142	114	97	85

**Table 1 : Droplet characteristic time response (SMD=12  $\mu$ m , slip velocity =10m/s).**

Objective comparison requires the normalization by reference value at atmospheric air density. Experimental and physical normalized characteristic lengths are plotted in figure 15.

Normalized characteristic length:

$$\text{Experimental } \bar{L}_i = \frac{L_{A_i}}{L_{A_{1,2}}}$$

$$\text{Physical } \bar{L}_{\tau p_i} = \frac{L_{\tau p_i}}{L_{\tau p_{1,2}}}$$

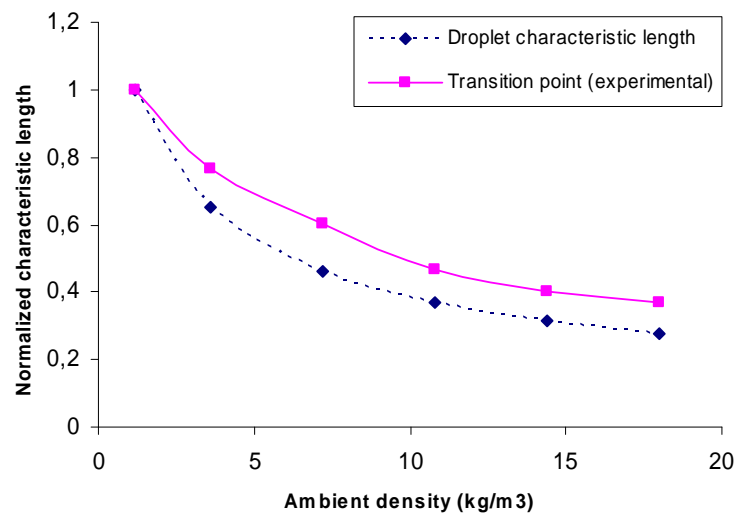


**Figure 15 : Density effect on transition point.**

Both curves are quickly decreasing from 1 to 5 kg/m<sub>3</sub> and then calm down. The observed decrease is due to an increase of drag forces, which are the main one applied on droplet. This force depends on the ambient density of the gas as well as the relative velocity of the droplet. The momentum exchange between the gas and the droplet, assimilated to a solid particle, is enhanced when ambient density increases, so that the droplet is stopped more rapidly. However, the hypothesis of an isolated spherical particle is valid if the continuum is weakly particle laden and become valid only a few distances from nozzle exit. Indeed, downward the transition point, the liquid jet (so called liquid sheet) is very dense so that multi droplet array should be taken into account. The drag force applied on a droplet in the wake of another one being less, the averaged penetration should be longer.

However, the tendency of both curves is well respected leading to the conclusion that a characteristic length based on the physical time response is apposite. This comment constitutes an interesting clue for the prediction of the air entrained mass flow rate model.

## 5. Summary and conclusions

As a mean of studying air / fuel mixture formation in gasoline direct injection engine, an accurate experimental PIV based setup has been implemented. The dense two-phase flow well adapted technique relies on Fluorescent PIV one and permits to study gaseous phase in the close vicinity of the spray edge. Due to the simultaneous attendance of both tracers and droplets in PIV images, classical treatment methods turned out to be unsatisfying. This is the reason why a new algorithm of post-treatment has been developed. This method based on various tests combination permits to eradicate most of wrong persistent vectors inside and outside of the spray and validate the use of ensemble averaged method.

Measurements have been carried out in the vicinity of the spray edge and used to compute the axial evolution of the cumulative air entrained mass flow rate  $\dot{m}_e$ . Density effect has been studied and  $\dot{m}_e$  is found to increase about 1200 % without saturation in the investigated range ( $\rho$  varying between  $1.2 \text{ kg/m}^3$  and  $18 \text{ kg/m}^3$ ). Good agreement is found with a one dimensional model that assumes a  $3/2$  and a  $5/6$  power law dependence of axial distance  $Z$  and density  $\rho$ , respectively, in the near field whereas a linear and a  $1/2$  power law of  $Z$  and  $\rho$  in the far field (like in variable density jet). The transition between the two regions depends on ambient density and appears more rapidly as  $\rho$  increase. Analyses of this result have been preformed in term of drop relaxation time (or length) and give interesting clue for the use of the model as a predictive one.

Further works are still in progress concerning single injection and aim at providing information on air entrainment mechanism as well as vortex formation as a function of:

- Lift effect
- Injection pressure effect
- Unsteady effect

## 6. Acknowledgements

The authors wish to acknowledge financial support from PSA, Siemens VDO Automotive and the Association Nationale de la recherche Technique (ANRT). The authors would also like to thank G. Couteau, M. Marchal and H. Ayroles for technical support.

## 7. References

1. Schwarz Ch, Schünemann E., Durst B., Fischer J. and Witt A., Potentials of the spray guided BMW DI Combustion System, SAE 2006-01-1265
2. Benatt F. G. S., Eisenklam P, Gazeous entrainment into axisymmetric liquid sprays. Journal of the Institute of Fuel [309], 1969.
3. Coghe A. , Cossali G.E. and Araneo, Gas entrainment in Diesel Sprays. International Conference on Thermo and Fluid Dynamic Processes in Diesel Engines, 2000.
4. Delay G., Analyse des écoulements transitoires dans les systèmes d'injection directe essence, effets sur l'entrainement d'air instationnaire du spray, PhD Thesis, INP Toulouse, France 2005.
5. Ghosh S., Hunt J. C. R. , Induced air velocity within droplet driven sprays. Proc. R. Soc. Lond. A 444, 1994.
6. Rottenkolber G. and al. Spray analysis of a gasoline direct injector by means of two-phase PIV. Experiments in Fluids, 2002.
7. Arbeau A, Bazile R, Charnay G, Gastaldi P, A new application of the particle image velocimetry (PIV) to the air entrainment in Gasoline Direct Injection spray, SAE Fuels & Lubricants Conference & Exhibition, 2004

8. Westerweel J. and Scarano F., Universal outlier detection for PIV data. *Experiments in Fluids*, 2005
9. Cossali G. E., An integral model for gas entrainment into full cone sprays. *J. Fluid Mech.*, Vol. 439 : 353-366, 2001.
10. Delay G, Arbeau A., Bazile R. and Charnay G., Experimental analysis of density effect on air entrainment in diesel and gasoline dense spray by PIV on fluorescent dyes. 6<sup>th</sup> World conference on Experimental Heat Transfert, Fluid Mechanics and Thermodynamics, 2005.
11. Riethmuller M., *La Velocimétrie par Image de Particules – PIV*, A.F.V.L, Ecole d'Autonome velocimétrie et granulométrie laser en mécanique des fluides, St Pierre d'Oleron, 1999
12. Scarano F. and Riethmuller M., Advances in iterative multigrid PIV image processing, *Experiments in Fluids* vol. [Supp.] S51-S60, 2000.